Q-Least Squares Reverse Time Migration with Viscoacoustic Deblurring Filters

Yuqing Chen[1] *, Gaurav Dutta*[1] *, Wei Dai*[2] *and Gerard T. Schuster*[1]
[1] *King Abdullah University of Science and Technology (KAUST), Thuwal 23955-6900, Kingdom of Saudi Arabia.*
[2] *Schlumberger*

SUMMARY

Viscoacoustic least-squares reverse time migration (Q-LSRTM) linearly inverts for the subsurface reflectivity model from lossy data. It can compensate for the amplitude loss and phase distortion in the migrated images because of the strong subsurface attenuation. However, the adjoint Q propagators used for backward propagating the residual data are also attenuative. Thus, the inverted images from Q-LSRTM are often observed to have lower resolution when compared to the benchmark acoustic LSRTM images from acoustic data. To increase the resolution and accelerate the convergence of Q-LSRTM, we propose using viscoacoustic deblurring filters as a preconditioner for Q-LSRTM. These filters can be estimated by matching a simulated migration image to its reference reflectivity model. Numerical tests on synthetic and field data demonstrate that Q-LSRTM combined with viscoacoustic deblurring filters can produce images with higher resolution and more balanced amplitudes when there is strong attenuation in the background medium. The proposed preconditioning method is also shown to improve the convergence rate of Q-LSRTM. These benefits only require the extra computational cost of constructing the deblurring filters, which is approximately no more than one migration of the data.

INTRODUCTION

Migration deconvolution (MD) is used to deblur migration images corrupted by artifacts due to coarse source and receiver sampling (Hu and Schuster, 1998), limited aperture width, strong velocity contrasts, and uneven subsurface illumination (Hu et al., 2001). Previous research on MD (Yu et al., 2006; Aoki and Schuster, 2009; Dai and Schuster, 2009; Dai et al., 2011) assumed a lossless background medium. However, strong subsurface attenuation can significantly distort the amplitudes and phases of seismic waves (Aki and Richards, 1980). In this case, conventional acoustic reverse time migration (RTM) and least-squares reverse time migration (LSRTM) cannot completely correct for the attenuation loss.

To account for attenuation, Q-LSRTM has been shown to compensate for the attenuation loss and produce images with more balanced amplitudes and accurately positioned reflectors than standard migration techniques (Dutta and Schuster, 2014; Dai et al., 2015; Sun et al., 2016). However, the inverted images from Q-LSRTM sometimes have lower resolution when compared to the original acoustic LSRTM images. This is because the adjoint Q propagators used for backpropagating the data residual are also attenuative. Hence, a large number of least-squares iterations are required to get the desired uplift in the image quality, which makes the Q-LSRTM technique computationally expensive when compared to standard RTM.

To mitigate these problems, we propose using viscoacoustic deblurring filters as a preconditioner for Q-LSRTM. A reference reflectivity model is first constructed using a uniform distribution of point scatterers while the background velocity and Q models are kept the same. The viscoacoustic data generated from these background models are then migrated by viscoacoustic reverse time migration (Q-RTM) to obtain a reference migration image. The viscoacoustic deblurring filters are then estimated for different parts of the migration image using local matching filters to transform the simulated migration image into its reference reflectivity model. These filters are then used as a preconditioner during the Q-LSRTM iterations.

This paper is divided into four sections. After the introduction, the second section presents the theory of Q-LSRTM with viscoacoustic deblurring filters. Numerical tests on synthetic and field data are then used to demonstrate the advantages of the proposed preconditioning method. The conclusions are in the last section.

THEORY

Strong subsurface attenuation can significantly distort the amplitudes and phases of seismic waves (Aki and Richards, 1980). To mitigate this problem, Q-LSRTM (Dutta and Schuster, 2014) was developed to generate migration images with more balanced amplitudes and accurately positioned reflectors than standard migration techniques. However, the inverted images from Q-LSRTM sometimes tend to have lower resolution when compared to the benchmark acoustic LSRTM images using lossless data. This is because the adjoint Q propagators used for backpropagating the data residual in Q-LSRTM are also attenuative.

This loss of resolution can be explained by analyzing the migration Green's function for a viscoacoustic medium. In a lossy medium, for a homogeneous medium with velocity v_0 and a monochromatic point source at $\mathbf{x_s} = (x_s, z_s)$ with angular frequency ω, the viscoacoustic Green's function $G(\mathbf{x}, \mathbf{x_s})$ is given by

$$G(\mathbf{x},\mathbf{x}_s) = \frac{1}{|\mathbf{x}_s-\mathbf{x}|}\overbrace{\exp\{\frac{i\omega|\mathbf{x}_s-\mathbf{x}|}{v_0\xi}\}}^{phase\ distortion}\quad\overbrace{\exp\{-\frac{\omega|\mathbf{x}_s-\mathbf{x}|}{2Qv_0\xi}\}}^{amplitude/frequency\ attenuation}, \tag{1}$$

where $\xi = [1+\frac{1}{\pi Q}(ln(\frac{\omega}{\omega_0}))][1+\frac{1}{4Q^2}]$. Q is the quality factor which is used to quantify the attenuation in the subsurface and ω_0 is the reference frequency (usually chosen to be the central

frequency of the source wavelet). The first exponential term is the phase distortion term and the second exponential term represents the amplitude/high-frequency loss term. Therefore, the viscoacoustic migration Green's function can be approximated by

$$\Gamma_Q = \int_\omega d\omega \sum_s \sum_r \frac{\exp\{i\frac{\omega}{v_0\xi}(rr - rr_0)\}\exp\{-\frac{\omega}{2Qv_0\xi}(rr + rr_0)\}}{|\mathbf{x_s}-\mathbf{x}|\cdot|\mathbf{x_r}-\mathbf{x}|\cdot|\mathbf{x_s}-\mathbf{x_0}|\cdot|\mathbf{x_r}-\mathbf{x_0}|}, \tag{2}$$

where $rr = |\mathbf{x_s}-\mathbf{x}| + |\mathbf{x_r}-\mathbf{x}|$ and $rr_0 = |\mathbf{x_s}-\mathbf{x_0}| + |\mathbf{x_r}-\mathbf{x_0}|$. Equation 2 shows that if viscoacoustic migration (i.e., Q-RTM) is used, the backward propagated receiver wavefield in Q-RTM is further attenuated because of the $\exp\{-\frac{\omega}{2Qv_0\xi}(rr_0)\}$ term on the RHS of equation 2. Thus, the inverted images from Q-LSRTM will have lower resolution when compared to the images computed by acoustic LSRTM on acoustic data.

To increase the resolution of the Q-LSRTM images and accelerate the convergence of the least-squares iterations, we propose the use of local viscoacoustic deblurring filters to approximate the inverse of the Hessian in a viscoacoustic medium. Assuming the SLS model (Christensen, 1982; Carcione et al., 1988; Blanch et al., 1995) and the Born approximation, the observed data $\mathbf{d}_Q$ can be represented as

$$\mathbf{d}_Q = \mathbf{L}_Q\mathbf{m}_0, \tag{3}$$

where $\mathbf{L}_Q$ is a linearized viscoacoustic modeling operator. The migration image $\mathbf{m}_{mig}$ is computed by applying the migration operator $\mathbf{L}_Q^\dagger$ to the lossy data as

$$\mathbf{m}_{mig} = \mathbf{L}_Q^\dagger\mathbf{d}_Q. \tag{4}$$

The viscoacoustic deblurring filters are estimated by defining a uniform distribution of point scatterers as the reference reflectivity model. The viscoacoustic synthetic data are generated using this reference reflectivity model and the background velocity and Q models. The data are then migrated by Q-RTM to obtain a reference Q-RTM image. Viscoacoustic deblurring filters for different subdomains of the Q-RTM image are then estimated using matching filters. The viscoacoustic deblurring filter for the ith local window is estimated in the space domain by solving the system of equations given by

$$[\mathbf{F}_Q]_i \otimes [\mathbf{L}_Q^\dagger\mathbf{L}_Q\mathbf{m}_{ref}]_i \approx [\mathbf{m}_{ref}]_i, \tag{5}$$

where $[\mathbf{F}_Q]_i$ and $[\mathbf{m}_{ref}]_i$ represent the viscoacoustic deblurring filter and reference reflectivity model in the ith local window, respectively. The symbol $\otimes$ here means 2D convolution. As the reference migration image is generated from the same source-receiver configuration as the original field experiment and by using the same velocity and Q models, the application of these deblurring filters to the migration image is an acceptable approximation to the true inverse Hessian operator $[\mathbf{L}_Q^\dagger\mathbf{L}_Q]^{-1}$.

The misfit function for Q-LSRTM is given by (Dutta and Schuster, 2014)

$$\varepsilon = \frac{1}{2}\|\mathbf{L}_Q\mathbf{m}^{(k)} - \mathbf{d}_Q^{obs}\|^2, \tag{6}$$

where $\mathbf{d}_Q^{obs}$ denotes the observed data that have suffered from attenuation, $\mathbf{m}^k$ represents the migration image at the k^{th} iteration and $\mathbf{L}_Q$ is the linearized viscoacoustic forward modeling operator. The Gauss-Newton gradient $\mathbf{g}^{(k)}$ for this misfit function is given by

$$\mathbf{g}^{(k)} = (\mathbf{L}_Q^\dagger\mathbf{L}_Q)\triangle\mathbf{m}^{(k)} = \mathbf{L}_Q^\dagger[\mathbf{L}_Q\mathbf{m}^{(k)} - \mathbf{d}_Q^{obs}]. \tag{7}$$

It can be seen from this equation that the gradient at each iteration $\mathbf{g}^{(k)}$ is a blurred version of the desired update $\Delta\mathbf{m}^{(k)}$ caused by the viscoacoustic migration Green's function $\mathbf{L}_Q^\dagger\mathbf{L}_Q$. Thus, a preconditioner for the gradient in equation 7 can be written as the deblurring approximation $[\mathbf{L}_Q^\dagger\mathbf{L}_Q]^{-1} \approx \mathbf{F}_Q$, so that the preconditioned gradient in equation 7 can be used in the iterative update equation

$$\mathbf{m}^{(k+1)} = \mathbf{m}^{(k)} - \alpha\mathbf{F}_Q \otimes (\mathbf{L}_Q^\dagger(\mathbf{L}_Q\mathbf{m}^{(k)} - \mathbf{d}_Q^{obs})), \tag{8}$$

where α is the step length.

NUMERICAL RESULTS

The effectiveness of Q-LSRTM with viscoacoustic deblurring filters is now demonstrated with synthetic and field data examples. The data are migrated using acoustic RTM, acoustic LSRTM, Q-RTM, Q-LSRTM and Q-LSRTM with viscoacoustic deblurring filters. The migration results in the same figure are compared at the same colorbar scale.

The preconditioned Q-LSRTM method is first tested on the Marmousi II model. Figure 1 shows the true velocity and Q models, respectively. A Ricker wavelet with a peak frequency of 15 Hz is used as the source wavelet. A fixed-spread acquisition geometry is used where there are 150 sources evenly distributed on the surface at an interval of 50 m. The data are recorded by 800 receivers for each shot uniformly distributed every 10 m on the surface.

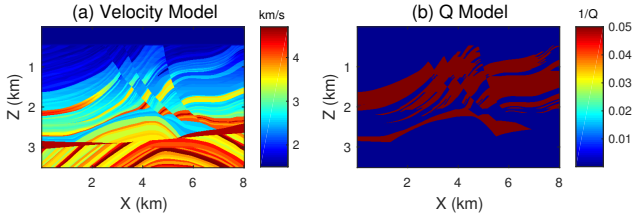

Figure 1: The Marmousi model: (a) true velocity model and (b) true Q model.

Conventional acoustic RTM and LSRTM images obtained from the viscoacoustic data are shown in Figures 2a and 2b, respectively. Both these images fail to recover the amplitudes of the reflectors at the deeper parts. The Q-LSRTM image, shown in Figure 2d, shows improvement in the deeper layers when

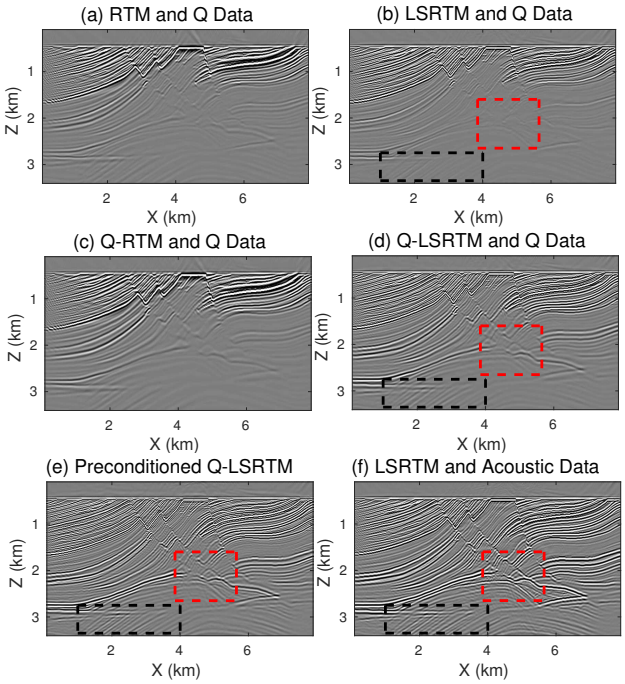

Figure 2: Comparison between images computed from viscoacoustic data by (a) acoustic RTM, (b) acoustic LSRTM, (c) Q-RTM, (d) Q-LSRTM, (e) Q-LSRTM using viscoacoustic deblurring filters as a preconditioner, where 20 least-squares iterations are carried out in all cases. (f) Acoustic LSRTM for lossless acoustic data, which is used as the benchmark image.

compared to the acoustic migration results. However, the Q-LSRTM image has lower resolution for the reflectors below the Q anomaly when compared to the benchmark acoustic LSRTM image, shown in Figure 2f, that has been obtained from acoustic data generated using the same velocity model in Figure 1a. The preconditioned Q-LSRTM image in Figure 2e computed with the viscoacoustic deblurring filters has better resolution when compared to the Q-LSRTM image in Figure 2d and better balanced amplitudes than the acoustic RTM and LSRTM images.

Magnified views of these images are compared in Figures 3 and 4, where the black arrows point to the areas in which noticeable improvements in resolution can be seen. Figure 3 shows the wavenumber spectrum of a vertical slice at $x = 3.11$ km in Figure 3. The wavenumber spectrum clearly shows the improvement in resolution with preconditioned Q-LSRTM, which is also confirmed in Figure 4e which shows the wavenumber spectrum of a vertical slice at $x = 5.13$ km in Figure 4. It is evident from these plots that the high-wavenumber details in the image are successfully recovered in the preconditioned Q-LSRTM image and these images have a similar resolution as the benchmark image obtained from applying acoustic LSRTM to lossless acoustic data.

The data residual as a function of iteration number for acoustic LSRTM, Q-LSRTM and preconditioned Q-LSRTM is plotted in Figure 5, where it can be seen that the convergence rate of the proposed Q-LSRTM method is much faster that the standard acoustic and Q-LSRTM methods.

For the field data example, we test our preconditioned Q-LSRTM

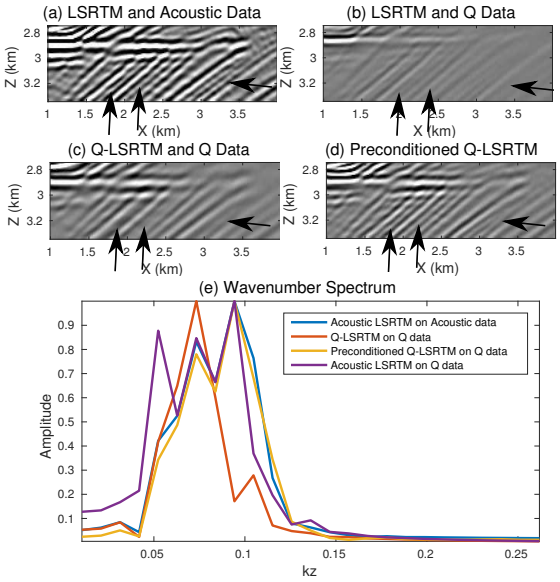

Figure 3: Magnified views of the black boxes in Figures 2b, 2d, 2e and 2f. The black arrows point to the areas in which improvements can be seen, and Figure 3e shows the k_z wavenumber spectrum of a vertical slice at $x = 3.11$ km in the above four pictures.

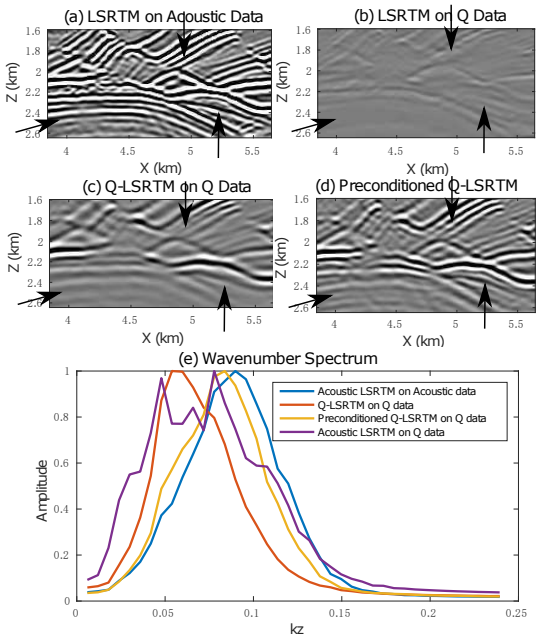

Figure 4: Magnified views of the red boxes in Figures 2b, 2d, 2e and 2f. The black arrows point to the areas in which improvements can be seen, and Figure 4e shows the k_z wavenumber spectrum of a vertical slice at $x = 5.13$ km in the above four pictures.

method on the Friendswood crosswell field data set. Two 305-m-deep cased wells separated by 183 m were used as the source and receiver wells. Downhole explosive charges were fired at intervals of 3 m from 305 m to 9 m in the source well, and the receiver well had 96 receivers placed at depths ranging from 293 m to 3 m. For these data, the migration velocity and Q models are shown in Figures 6a and 6b, respectively. The migration velocity model is estimated by early-arrival waveform inversion and the migration Q model is estimated by wave-equation Q tomography (Dutta, 2016; Dutta

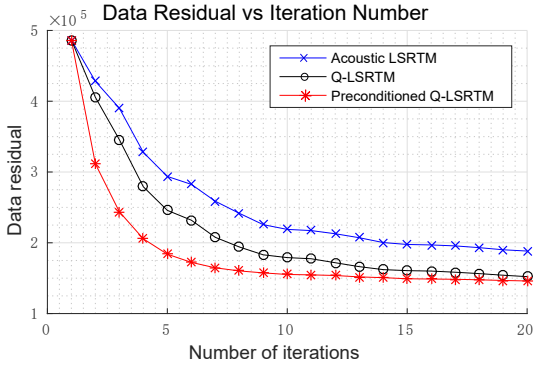

Figure 5: Data residual vs number of iterations for acoustic LSRTM, Q-LSRTM and preconditioned Q-LSRTM applied to data associated with the Marmousi II model.

and Schuster, 2016).

The comparison between the acoustic LSRTM and Q-LSRTM images after 20 iterations are shown in Figures 7a and 7b, respectively. Similar to the synthetic examples, the amplitudes are more balanced in the Q-LSRTM image in Figure 7d than in the acoustic RTM and LSRTM images in Figures 7a and 7b, respectively. However, the resolution of this image is lower than the acoustic LSRTM image. The preconditioned Q-LSRTM image is shown in Figure 7e which has better resolution at depths of 10-80 m as well as better balanced amplitudes than the acoustic RTM and LSRTM images. The black arrows in the magnified views of these images in Figure 8 validate the same.

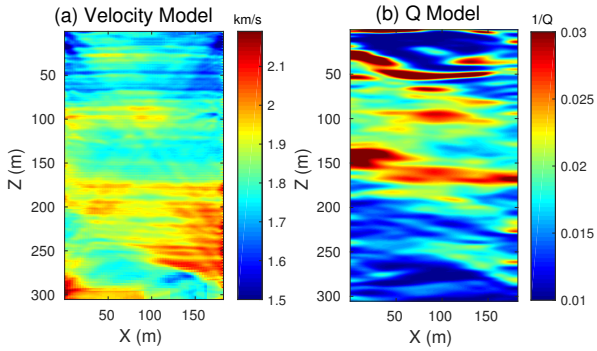

Figure 6: (a) The estimated migration velocity and (b) Q models for the Friendswood cross-well data.

SUMMARY AND CONCLUSIONS

A preconditioned Q-LSRTM method is presented that uses visco-acoustic deblurring filters to compensate for the amplitude and resolution losses due to strong subsurface attenuation. Numerical tests on synthetic and field data validate that the proposed preconditioning method mitigates the problem of low resolution associated with standard Q-LSRTM and can produce images with better balanced amplitudes and better resolution than acoustic RTM and LSRTM. The proposed preconditioning method is also shown to significantly increase the convergence rate of Q-LSRTM.

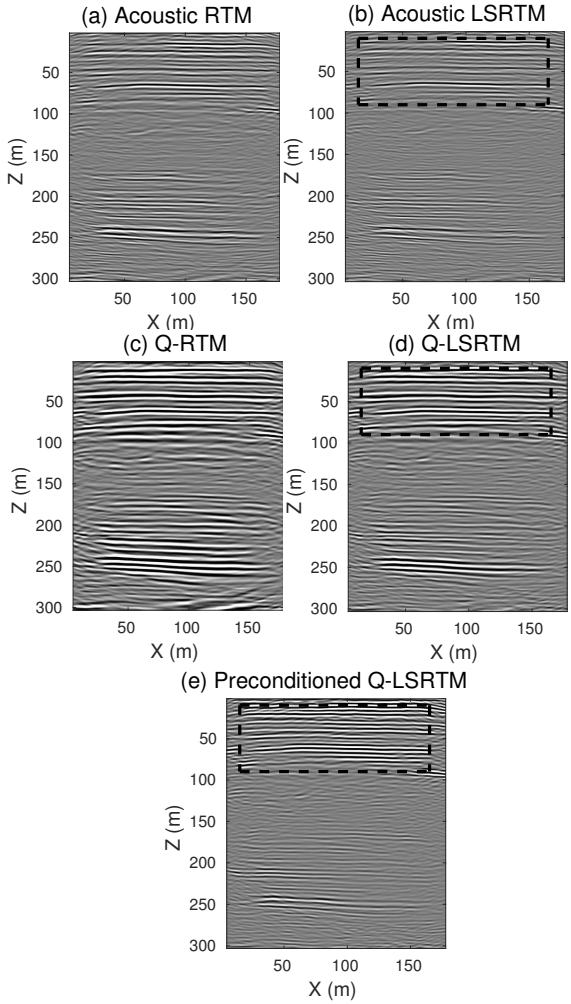

Figure 7: Comparison between images from (a) acoustic RTM, (b) acoustic LSRTM, (c) Q-RTM, (d) Q-LSRTM and (e) preconditioned Q-LSRTM. Twenty iterations are carried out in b), d) and e).

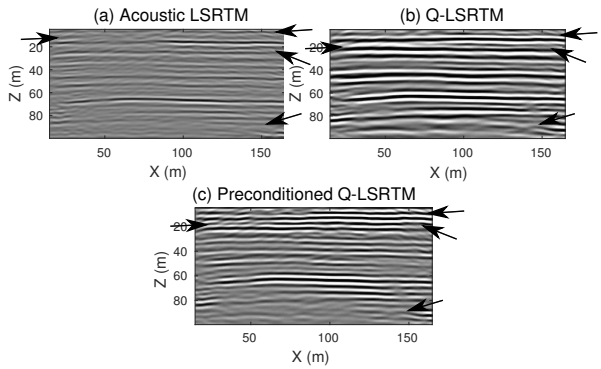

Figure 8: Magnified views of the black boxes in Figure 7. The black arrows point to the reflectors where the improvement in resolution can be seen from the preconditioned Q-LSRTM method.

ACKNOWLEDGMENTS

We thank the sponsors of the CSIM consortium, the KAUST Supercomputing Laboratory and IT Research Computing Group.

EDITED REFERENCES

Note: This reference list is a copyedited version of the reference list submitted by the author. Reference lists for the 2017 SEG Technical Program Expanded Abstracts have been copyedited so that references provided with the online metadata for each paper will achieve a high degree of linking to cited sources that appear on the Web.

REFERENCES

Aki, K., and P. G. Richards, 1980, Quantitative seismology: Freeman Publication Co.

Aoki, N., and G. T. Schuster, 2009, Fast least-squares migration with a deblurring filter: Geophysics, **74**, WCA83–WCA93, http://doi.org/10.1190/1.3155162.

Blanch, J. O., J. O. Robertsson, and W. W. Symes, 1995, Modeling of a constant Q: Methodology and algorithm for an efficient and optimally inexpensive viscoelastic technique: Geophysics, **60**, 176–184, http://doi.org/10.1190/1.1443744.

Carcione, J. M., D. Kosloff, and R. Kosloff, 1988, Wave propagation simulation in a linear viscoacoustic medium: Geophysical Journal International, **93**, 393–401, http://doi.org/10.1111/j.1365-246X.1988.tb02010.x.

Christensen, R., 1982, Theory of viscoelasticity: an introduction: Academic Press.

Dai, W., and G. T. Schuster, 2009, Least-squares migration of simultaneous sources data with a deblurring filter: 79th Annual International Meeting, SEG, Expanded Abstracts, 2990–2994, https://doi.org/10.1190/geo2010-0159.1.

Dai, W., X. Wang, and G. T. Schuster, 2011, Least-squares migration of multisource data with a deblurring filter: Geophysics, **76**, R135–R146, http://doi.org/10.1190/geo2010-0159.1.

Dai, W., Z. Xu, and R. Coates, 2015, Least-squares reverse-time migration for visco-acoustic media: 85th Annual International Meeting, SEG, Expanded Abstracts, 3387–3391, https://doi.org/10.1190/segam2015-5922472.1.

Dutta, G., 2016, Skeletonized wave-equation inversion for Q: 86th Annual International Meeting, SEG, Expanded Abstracts, 3618–3623.

Dutta, G., and G. T. Schuster, 2014, Attenuation compensation for least-squares reverse time migration using the viscoacoustic-wave equation: Geophysics, **79**, S251–S262, http://doi.org/10.1190/geo2013-0414.1.

Dutta, G., and G. T. Schuster, 2016, Wave-equation Q tomography: Geophysics, **81**, R471–R484, http://doi.org/10.1190/geo2016-0081.1.

Hu, J., and G. T. Schuster, 1998, Migration deconvolution: SPIE International Symposium on Optical Science, Engineering, and Instrumentation: International Society for Optics and Photonics, 118–124.

Hu, J., G. T. Schuster, and P. A. Valasek, 2001, Poststack migration deconvolution: Geophysics, **66**, 939–952, http://doi.org/10.1190/1.1444984.

Sun, J., S. Fomel, T. Zhu, and J. Hu, 2016, Q-compensated least-squares reverse time migration using low-rank one-step wave extrapolation: Geophysics, **81**, S271–S279, http://doi.org/10.1190/geo2015-0520.1.

Yu, J., J. Hu, G. T. Schuster, and R. Estill, 2006, Prestack migration deconvolution: Geophysics, **71**, S53–S62, http://doi.org/10.1190/1.2187783.